Acta Cryst. (1995). B**51**, 1021–1028

The Crystal Structure of Waxes

BY DOUGLAS L. DORSET

Electron Diffraction Department, Hauptman–Woodward Medical Research Institute, Inc., 73 High Street, Buffalo, NY 14203-1196, USA

(*Received* 28 *October* 1994; *accepted* 21 *April* 1995)

Abstract

Quantitative electron crystallographic studies have been carried out on epitaxially oriented multi-component waxes. Intensities from two paraffin-based samples, an artificial six-component medium wax (equimolar distribution of chain lengths) and a petroleum-based wax (Gaussian distribution of chain lengths) have been used to determine their crystal structures. As found earlier for binary paraffin solid solutions, differences in molecular volume are compensated by longitudinal molecular shifts within individual lamellae. Nevertheless, each lamellar surface must remain flat enough, and with enough crystallographic order intact, to nucleate the next lamella, thus accounting for the observed long-range correlation in these crystals. Recrystallized beeswax also has a layer packing somewhat similar to the paraffin waxes. However, in this case, the lamellar order is 'frustrated' so that a certain amount of 'nematically' ordered material must be present, spanning the nascent lamellar interfaces.

Introduction

Polydisperse combinations of linear molecules are often found in biologically and commercially significant materials, ranging from the lipids to synthetic polymers. Multicomponent paraffin solid solutions, themselves, have been significant for the study of petroleum wax crystallization, as a model for insect and plant cuticle waxes and as a model for polydisperse polyethylene lamellae.

Crystallographically, the description of such polydisperse linear-chain combinations is not well advanced. Progress has been made recently in the study of binary *n*-paraffin solids in the form of single crystals. Low-angle X-ray diffraction measurements had often been made on such samples (Mnyukh, 1960; Fischer, 1971; Asbach, Geiger & Wilke, 1979; Craievich, Doucet & Denicolo, 1984) and, more recently, on polydisperse solids (Asbach & Kilian, 1991; Basson & Reynhardt, 1992). However, the first single-crystal characterization of an *n*-paraffin binary solid solution was reported only two decades ago (Lüth, Nyburg, Robinson & Scott, 1974). In this qualitative description, it was proposed that the co-packing of dissimilar chain lengths was compensated by longitudinal molecular disorder in individual lamellae. Vibrational spectroscopic (Maroncelli, Strauss & Snyder, 1985; Kim, Strauss & Snyder, 1989) as well as NMR measurements (Basson & Reynhardt, 1991) established that conformational disorder near the chain ends was also important for minimizing the average nonoverlapping volume. Recent quantitative crystal-structure analyses of such solid solutions, based on electron (Dorset, 1990*a*) or X-ray diffraction (Gerson & Nyburg, 1994) intensities, support the longitudinal disorder model.

In an earlier electron diffraction study of binary paraffin combinations (Dorset, 1987), it was found that similar patterns could also be obtained from an oriented commercial petroleum wax. In this paper, the study of paraffin-based multicomponent waxes is extended to find a more quantitative model for the molecular packing. A similar characterization of a natural beeswax is then compared with the paraffin wax model.

Materials and methods

Materials

Pure paraffins used to construct several model waxes have been listed in an earlier paper (Dorset, 1990*b*), along with their individual purities and thermal properties. Asymmetric long-chain esters (>99% pure, NuChekPrep, Elysian MN), used as ingredients for a model beeswax, included the behenyl esters of myristic acid, palmitic acid, stearic acid and arachidonic acid, with respective carbon chain lengths: C36, C38, C40 and C42.

Model waxes (Table 1) were formed from individual ingredients by weighing into a vial and then fusing together on a hot plate. After cooling, the solid was broken up, re-mixed and re-melted to give a homogeneous solid solution (indicated initially by single melting endotherms in DSC scans) after re-cooling. 'Natural' waxes were taken directly from commercial sources. A typical commercial petroleum wax was obtained from a paraffin birthday candle. Typical of petroleum waxes, it would have a Gaussian distribution of chain components (Tegelaar, Matthezing, Jansen, Horsfield & de Leeuw, 1989). Honeycomb beeswax (*Apis mellifera*) was obtained from a local apiary and was received as a yellow pigmented cake. Its very complicated composition has been discussed by various authors

Table 1. *Wax samples*

Code	Composition	DSC melting point (K)
Medium wax (MW2636)	Equimolar: C26, C28, C30, C32, C34, C36	339.0
Behenyl wax (BEHWX)	Equimolar behenyl: myristate, palmitate, stearate, arachidate	339.4
Petroleum wax (CANWX)	Paraffin candle, *n*-paraffins	329.2
Beeswax	Honeycomb: Long-chain esters, fatty alcohols, fatty acids, *n*-paraffins	337.8
Artificial beeswax	1:2 MW2636/BEHWX	334.8

(Downing, Kranz, Lamberton, Murray & Redcliffe, 1961; Stransky & Streibl, 1971; Stransky, Streibl & Kubelka, 1971; Tulloch, 1970, 1971, 1972) and a mass spectral analysis of component chain lengths (Tulloch, 1972) was used to guide the construction of the beeswax model listed in Table 1.

For electron diffraction analyses, typical crystals with long chains normal to the major crystal face were grown by evaporation from dilute light petroleum solution. The more useful orthogonal projection onto the chain axes was achieved by epitaxial orientation on benzoic acid to form microcrystals so that the chain axes are nucleated to lie parallel to the major (100) crystal face (Wittmann, Hodge & Lotz, 1983; Dorset, Hanlon & Karet, 1989).

Electron diffraction structure analysis

Two instruments were used for selected-area electron diffraction studies: at 100 kV (selected area diameter *ca* 10 μm), a JEOL JEM-100CX II electron microscope and at 1000 kV (selected area diameter between 1.0 and 3.5 μm), a AEI EM7 high-voltage electron microscope. The usual precautions were taken to minimize radiation damage to the specimens (Dorset, 1994, 1995). After densitometry of the diffraction films (on Kodak DEF-5 film at 100 kV and Dupont Cronex at 1000 kV), intensities were measured as described earlier (Dorset, 1994). During the experiments at 100 kV, the samples could be heated with a temperature-controlled specimen stage (Gatan model 626).

The crystal structures were determined from the measured intensity data by direct methods. For solution crystallized samples (*hk*0 data), this procedure was originally described by Dorset & Hauptman (1976). From this analysis, the lateral packing of the $O_\perp$ subcell (Abrahamsson, Dahlén, Löfgren & Pascher, 1978) is obtained (Dorset, 1976) with cell constants $a_s = 7.42$, $b_s = 4.96$, $o_s = 2.55$ Å, space group *Pnam*. For epitaxially oriented samples (0*kl* patterns), the space group is either $Pna2_1$ or $A2_1am$ if the average layer, respectively, resembles the crystal structure of an even- or odd-chain paraffin. [Actually, the monoclinic space group *Aa* was also proposed for this particular polymorph of odd-chain paraffins (Piesczek, Strobl & Malzahn, 1974). When $\beta \approx 90°$ (so that differences in d^*_{00l} cannot be discerned), the monoclinic and orthorhombic space groups are indistinguishable in this projection.] From the indices of the most intense 01*l* reflections, the apparent carbon number *m* of the average lamellar layer is obtained from $l = m$, $m + 2$, as if it were a pure paraffin n-C_mH_{2m+2} (see Dorset, 1987). As discussed earlier (Dorset, 1987), the corresponding lamellar repeat agrees well with the values listed by Nyburg & Potworoski (1973), *i.e.* $c/2 = (1.273m + 1.875)$ Å. Although the two space groups are noncentrosymmetric, fitting a centrosymmetric subcell into these two space groups requires the phases of 0*kl* reflections to have values near $\pm\pi/2$ when $k = 2n + 1$ and near 0, π when $k = 2n$. As shown earlier (Dorset & Zemlin, 1990; Dorset & Zhang, 1991; Dorset, 1990*a*), this simplifies the structure determination by symbolic addition, so that a useful potential map can be obtained when centrosymmetric phases are generated. For calculation of structure factors, Doyle–Turner (Doyle & Turner, 1968) electron scattering factors were used. No corrections were made for dynamical scattering since the intensities used for structure analysis were recorded at 1000 kV.

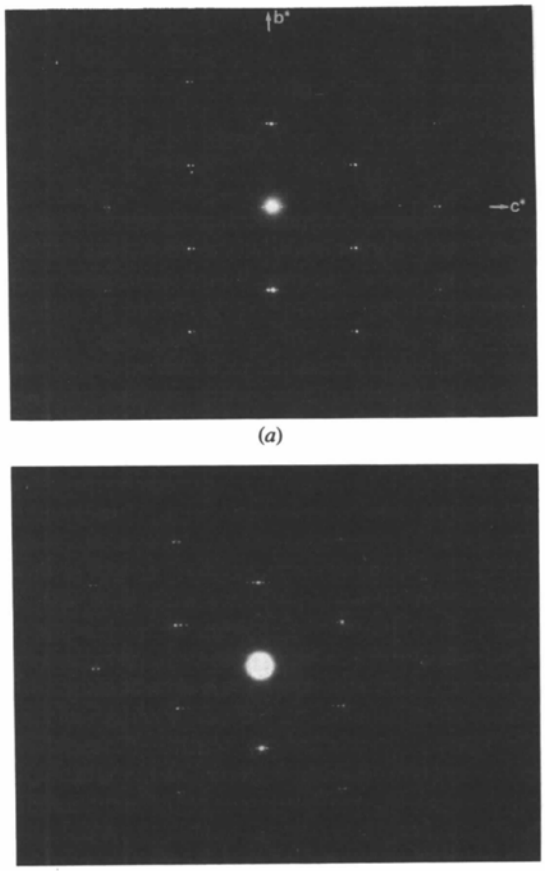

(*a*)

(*b*)

Fig. 1. Electron diffraction patterns (0*kl*) from paraffin-based multicomponent waxes epitaxially oriented on benzoic acid. (*a*) Medium wax (MW2636) from six even-chain *n*-paraffins from n-$C_{26}H_{54}$ to n-$C_{36}H_{74}$ in equimolar proportions. (*b*) Petroleum wax (CANWX) from a paraffin birthday candle.

Results

Paraffin waxes

Medium wax (*MW*2636). Electron diffraction patterns from epitaxially oriented samples of the artificial medium wax MW2636 show that the structure diffracts to very high resolution (0.75 Å) and that the microcrystalline regions are uniformly oriented (Fig. 1*a*). Indices of the 0*kl* reflections (see Dorset, 1987) indicate that contiguous microcrystalline areas, on average, mimic the crystal structures of either n-$C_{32}H_{66}$ or n-$C_{33}H_{68}$, with the latter being slightly more abundant. Following the work of Lüth, Nyburg, Robinson & Scott (1974), the orthorhombic space group for the odd-chain packing is $A2_1am$ (or *Aa*, as indicated above), with cell constants: $a = 7.42$, $b = 4.96$, $c = 87.94$ Å [the lamellar repeat to n-$C_{33}H_{68}$, given by Nyburg & Potworowski (1973) is $c/2 = 43.89$ Å]. The plane group of the [100] projection is *cm*. Thus, the origin can be placed anywhere along the mirror parallel to **c** in this plane group.

After direct methods were used to assign phase values (through two algebraic ambiguities) to 16 reflections, one potential map was generated (after permutation of values for the symbols; Fig. 2*b*) that depicted the carbon positions within each lamella of the bilamellar unit cell. It

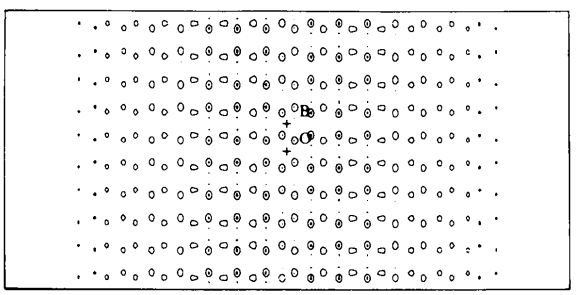

(*a*)

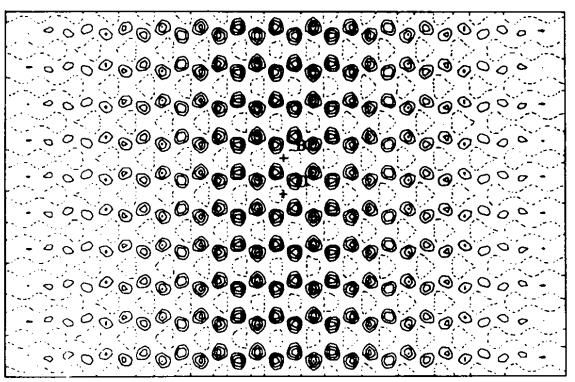

(*b*)

Fig. 2. Initial potential maps for the paraffin waxes after direct phase determination. In each case, only a single lamella of the bilamellar unit cell in space group $A2_1am$ is shown (see also Fig. 3). The origin on plane group *cm*, which must lie on the mirror, is arbitrarily placed near the lamellar center (the result of the direct phase determination). Peaks represent carbon positions and are weighted approximately by their occupancy in the lamella. (*a*) CANWX and (*b*) MW2636.

Table 2. *C-atom coordinates for MW*2636

y	z	Occupancy
0.190	0.0179	0.50
0.309	0.0324	0.79
0.190	0.0470	0.82
0.309	0.0615	0.85
0.190	0.0760	0.87
0.309	0.0905	0.89
0.190	0.1050	0.91
0.309	0.1196	0.91
0.190	0.1341	0.94
0.309	0.1486	0.95
0.190	0.1631	0.96
0.309	0.1776	0.99
0.190	0.1921	1.00
0.309	0.2066	1.00
0.190	0.2212	1.00
0.309	0.2357	1.00
0.190	0.2502	1.00
0.309	0.2647	1.00
0.190	0.2792	1.00
0.309	0.2938	1.00
0.190	0.3083	1.00
0.309	0.3228	0.99
0.190	0.3373	0.96
0.309	0.3518	0.95
0.190	0.3664	0.94
0.309	0.3809	0.91
0.190	0.3954	0.91
0.309	0.4092	0.89
0.190	0.4244	0.87
0.309	0.4390	0.85
0.190	0.4535	0.82
0.309	0.4680	0.79
0.190	0.4825	0.50

was clear from the map that an occupancy factor was required to account for the co-mixing of the various components in the solid solution, much as it was in earlier studies (Lüth, Nyburg, Robinson & Scott, 1974; Dorset, 1990*a*; Gerson & Nyberg, 1994). That is to say, because of translational adjustments of molecular positions in each layer along the long unit-cell axis, the atomic occupancies at the chain ends have an approximate Gaussian fall-off, reaching a maximum value at the chain centers.

Although not all the carbon positions are found in the initial potential map (Fig. 2*b*), it was assumed that the average crystal structure was that indicated by the 0*kl* indices, *i.e.* n-$C_{33}H_{68}$. When theoretical hydrogen positions are assigned to each carbon, a kinematical $R = 0.46$ is calculated (plane group *cm*) when all atoms are assigned unit weights and some of the enhanced resolution of the 00*l* row is included. A somewhat more reasonable fit to the observed data is obtained when the atomic occupancies found earlier for a 1:1 paraffin solid solution (Dorset, 1990*a*) are employed (Table 2), *i.e.* $R = 0.30$, when $B_C = 2.0$, $B_H = 4.0$ Å^2 (Table 3). Secondary scattering perturbations (Cowley, Rees & Spink, 1951), detected in electron diffraction patterns from similar microcrystalline paraffins (Hu, Dorset & Moss, 1989), were judged to affect the current data set, because the agreement between calculated and observed data is actually better when lower isotropic temperature factors were used in the structure factor calculation with this model. Correction for this type of multiple scattering

Table 3. *Observed and calculated structure factors for MW2636*

hkl	$\|F_o\|$	$\|F_c\|$	$\|F_c\|_{corr}$	*hkl*	$\|F_o\|$	$\|F_c\|$	$\|F_c\|_{corr}$
002	0.81	0.85	0.70	02,66	0.22	0.09	0.17
004	0.47	0.45	0.37	02,68	0.46	0.42	0.46
006	0.25	0.37	0.29	02,70	0.44	0.34	0.42
00,66	0.24	0.23	0.24	03,31	0.18	0.16	0.18
00,68	0.57	0.99	0.80	03,33	0.47	0.43	0.42
00,70	0.69	0.79	0.68	03,35	0.80	0.86	0.78
00,72	0.20	0.21	0.19	03,37	0.22	0.09	0.15
01,31	0.25	0.27	0.26	03,103	0.18	0.18	0.21
01,33	0.47	0.69	0.63	03,105	0.18	0.06	0.11
01,35	0.87	1.33	1.13	040	0.25	0.31	0.54
01,37	0.25	0.14	0.22	042	0.20	0.03	0.15
01,103	0.18	0.15	0.25	044	0.18	0.02	0.06
01,105	0.18	0.04	0.16	04,68	0.26	0.08	0.19
020	1.92	2.08	1.63	04,70	0.30	0.06	0.20
022	0.35	0.23	0.34	05,33	0.16	0.21	0.21
024	0.29	0.12	0.16	05,35	0.22	0.43	0.41

greatly improves the agreement ($R = 0.21$). The average crystal structure is drawn schematically in Fig. 3(*a*).

Petroleum wax (CANWX). When epitaxially oriented, the wax sample taken from a paraffin candle also diffracts electrons to high resolution (0.92 Å). Sharpness of the diffraction maxima again denotes uniform orientation within each microarea (Fig. 1*b*). Indices of the 0*kl* diffraction patterns reveal that the average lamellar structure is much more sharply distributed around a single crystal structure, n-$C_{29}H_{60}$. The orthorhombic space group is again $A2_1am$ (or Aa) with unit-cell constants: $a = 7.42$, $b = 4.96$, $c = 76.58$ Å. [The lamellar spacing for n-$C_{29}H_{60}$ predicted by Nyburg & Potworowski (1973) is $c/2 = 38.79$ Å.]

Symbolic addition assigns phase values for 13 of 22 unique observed reflections *via* two algebraic unknowns. After permutation of these unknown values, a potential map is observed (Fig. 2*a*), wherein 28 of 29 possible carbon positions are located. Again, the need for a decreasing occupancy factor to model the chain ends is apparent from this map.

If, as justified by the above measurements, the crystal structure of n-$C_{29}H_{60}$ is used as the basis for the structure determination, then, if both carbon and hydrogen positions are used for the structure factor calculation with unit occupancies, $R = 0.44$, when $B_C = 3.0$, $B_H = 4.0$ Å^2. When the three positions at the chain ends are assigned weights: 0.25, 0.50 and 0.75 (Table 4), the agreement improves to $R = 0.24$ (Table 5). Only a slight

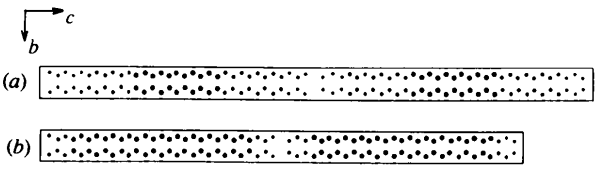

Fig. 3. Schematic representation of paraffin wax crystal structures where atomic radii denote decreasing occupancy factors. In comparison to Fig. 2, the origin is now placed between the lamellae, typical of paraffin crystal structure representations. (*a*) MW2636, as an average n-$C_{33}H_{68}$ structure, and (*b*) CANWX, as an average n-$C_{29}H_{60}$ structure.

Table 4. *C-atom coordinates for CANWX*

y	*z*	Occupancy
0.190	0.0203	0.25
0.309	0.0368	0.50
0.190	0.0532	0.75
0.309	0.0696	1.00
0.190	0.0861	1.00
0.309	0.1024	1.00
0.190	0.1189	1.00
0.309	0.1353	1.00
0.190	0.1517	1.00
0.309	0.1682	1.00
0.190	0.1846	1.00
0.309	0.2010	1.00
0.190	0.2175	1.00
0.309	0.2340	1.00
0.190	0.2503	1.00
0.309	0.2668	1.00
0.190	0.2833	1.00
0.309	0.2997	1.00
0.190	0.3161	[illegible]
0.309	0.3326	[illegible]
0.190	0.3491	[illegible]
0.309	0.3655	1.00
0.190	0.3839	1.00
0.309	0.3983	1.00
0.190	0.4147	1.00
0.309	0.4311	1.00
0.190	0.4475	0.75
0.309	0.4640	0.50
0.190	0.4840	0.25

Table 5. *Observed and calculated structure factors for CANWX*

hkl	$\|F_o\|$	$\|F_c\|$	*hkl*	$\|F_o\|$	$\|F_c\|$
002	0.85	1.25	022	0.30	0.33
004	0.79	1.03	024	0.20	0.27
006	0.68	0.73	02,58	0.35	0.08
008	0.46	0.42	02,60	0.36	0.38
00,58	0.83	0.20	03,27	0.18	0.19
00,60	0.75	0.97	03,29	0.44	0.45
01,25	0.26	0.18	03,31	0.68	0.79
01,27	0.37	0.34	040	0.36	0.32
01,29	0.71	0.79	042	0.19	0.05
01,31	1.13	1.36	05,29	0.23	0.20
020	2.39	2.13	05,31	0.30	0.36

improvement is seen ($R = 0.23$) when a correction is made for secondary scattering. A schematic representation of this average crystal structure is given in Fig. 3(*b*).

Honeycomb wax. Although thin microcrystals of yellow beeswax grown from dilute solution in light petroleum do not have well developed habits, the *hk*0 electron diffraction patterns from them (Fig. 4) are identical to those found for all the multi-component paraffin waxes considered in this study. In agreement with powder X-ray studies of beeswax (Basson & Reynhardt, 1988), the characteristic pattern from the orthorhombic perpendicular methylene subcell is observed, with lateral cell constants $a_s = 7.58$, $b_s = 5.08$ Å. When single crystals of the beeswax were heated in the electron microscope, there was only a slight expansion of the axial ratio a_s/b_s before the melting point, *i.e.* there is no rotator phase. This behavior is characteristic of *e.g.* pure even-chain paraffins when the chain length is longer than 38 carbons (Dorset, Alamo & Mandelkern, 1992).

Epitaxially oriented beeswax produces two types of $0kl$ diffraction pattern. In one case, the most intense reflections would closely resemble the pattern from polyethylene (Hu & Dorset, 1989), as shown in Fig. 5(*a*). Sometimes, however, the intense $01l$ reflection was found to be split, but the high resolution $00l$ reflection was never split (Fig. 5*b*). In all cases, low-angle 'lamellar' reflections are also observed in these patterns (Fig. 5*c*) with fairly consistent spacing, $c/2 = 65.8\ (7)$ Å. Comparing this lamellar distance to the split $01l$ reflections, it is found that the $l = m,\ m+2$ rule seen for the *n*-paraffins and their solid solutions (Dorset, 1987) is no longer obeyed. Instead, the relationship $l = m,\ m+3$ is found where $m = 51$ is most frequently observed. Using the Nyburg & Potworowski (1973) formula above, the predicted lamellar distance for n-$C_{51}H_{104}$ is $c/2 = 66.8$ Å, *i.e.* very close to the measured spacing.

If the combined $hk0$ and $0kl$ intensities from beeswax (however, only those from patterns of the form shown in Fig. 5*a*) were compared to a polyethylene model (Table 6), then a reasonable fit to the experimental data could be found (Table 7) when a strong anisotropic component was imposed along the chain axis. That is to say, $R = 0.26$, when $B_{C(1,2)} = 1.0$, $B_{H(1,2)} = 2.0$, $B_{C(3)} = 7.0$, $B_{H(3)} = 9.0$ Å^2, where the major ellipsoid axes were defined to lie along the unit-cell axes. Evidence for this translational component has also been detected in pure *n*-paraffins (Dorset, Hu & Jäger, 1991).

Because of a postulated role of volatile components in this wax (Basson & Reynhardt, 1988), the influence of high vacuum on the solid was tested by placing the bulk solid under 10^{-5} Torr for several days. No change in the melting point was found, however. Our measured value (Table 1) agrees well with earlier surveys of Canadian beeswaxes (Tulloch & Hoffman, 1972). Also, a low-angle X-ray measurement ($d_{002} = 64$ Å) of wax from the honeycomb is in reasonable agreement with the electron diffraction measurements made *in vacuo*.

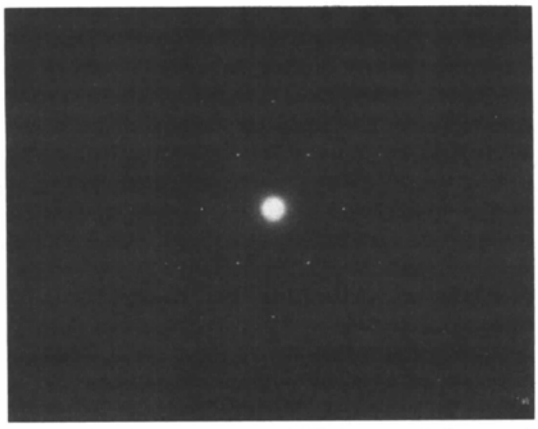

Fig. 4. Electron diffraction pattern ($hk0$) from a solution-crystallized beeswax lamella. The pattern is characteristic of the orthorhombic perpendicular ($O_\perp$) methylene subcell.

Beeswax model. Following the compositional distribution given by Tulloch (1972), an attempt was made to model beeswax with a co-mixture of shorter alkanes (HW2636) with the behenyl wax esters (BEHWX) to form a solid solution of 10 components. As shown in Table 1, the melting point is similar to that of natural beeswax. (An attempt to construct a model beeswax with

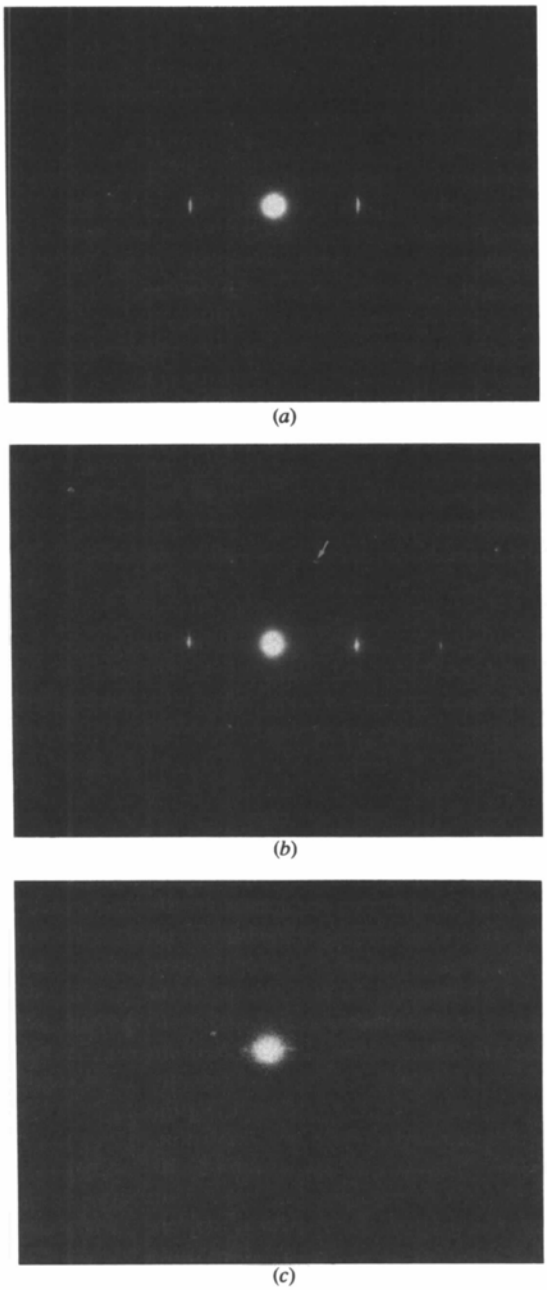

Fig. 5. Electron diffraction patterns ($0kl$) from beeswax epitaxially oriented on benzoic acid. (*a*) All intense reflections resemble the diffraction pattern from polyethylene; (*b*) intense $01l$ reflections are split (arrow); (*c*) low-angle 'lamellar' reflections observed in either (*a*) or (*b*) patterns.

Table 6. *Atomic coordinates for the orthorhombic perpendicular subcell*

	x	*y*	*z*
C	0.038	0.065	0.25
H1	0.179	0.049	0.25
H2	0.010	0.273	0.25

Table 7. *Observed and calculated structure factors for beeswax subcell data*

hkl	$\|F_o\|$	$\|F_c\|$	*hkl*	$\|F_o\|$	$\|F_c\|$
200	1.35	1.57	420	0.38	0.12
400	0.60	0.65	520	0.27	0.29
600	0.31	0.22	130	0.50	0.34
110	1.45	1.63	230	0.37	0.35
210	0.46	0.37	330	0.33	0.12
310	0.74	0.52	430	0.28	0.27
410	0.38	0.26	002	0.18	0.24
510	0.33	0.27	011	0.34	0.57
020	0.91	0.81	022	0.13	0.10
120	0.42	0.32	031	0.28	0.41
220	0.66	0.32	040	0.31	0.07
320	0.40	0.36			

an equivalent longer chain-length polydisperse paraffin component was not successful, since the melting point was 20° higher than that considered here.)

Electron diffraction studies of epitaxially oriented BEHWX indicate that the wax ester solid solution crystallizes as if it is an orthorhombic paraffin, in agreement with powder diffraction measurements made on pure asymmetric wax esters by Aleby, Fischmeister & Iyenger (1971). Indices of the 0*kl* patterns reveal that the structures resemble *n*-$C_{40}H_{82}$, *n*-$C_{41}H_{84}$ or *n*-$C_{42}H_{86}$, in space group $Pca2_1$ for the quasi-even-chain lamellae and $A2_1am$ (or *Aa*) for the odd.

Despite the similarity of peak melting points, however, there is no close structural resemblance between the artificial beeswax and the natural product. When 0*kl* patterns of the artificial beeswax are indexed, the average lamellar packing resembles most often the structure of *n*-$C_{38}H_{78}$, an average layer much thinner than found for honeycomb beeswax. The intense outer 00*l* reflections and 01*l* reflections corresponding to the major polyethylene diffraction positions in this projection are always split, so that the lamellae are well defined. Thus, the artificial beeswax closely resembles the two paraffin-based waxes described above.

Discussion

The analysis of *n*-paraffin multi-component solid solutions, either as artificially compounded mixtures or as a commercial product derived from a petroleum source, demonstrates that there is, if any, very little structural difference in these polydisperse solids from the simple *binary solid solutions*. As also found for the binary solid solutions (Dorset, 1987), there is a distribution of local orthorhombic crystal structures from microarea to microarea and these mimic, on average, the lamellar packing of either an even- or an odd-chain paraffin. The co-packing of various chain lengths in a single lamella requires that some mechanism must compensate for the molecular volume differences. The methylene subcell packing itself is not disordered appreciably, so that these groups are always well-aligned within a chain layer. The longitudinal molecular translational disorder component for individual chains included in the structure analyses of binary and now multi-component solutions accounts, therefore, for the phenomenological fall-off of chain-end atomic occupancy. Since this approximately Gaussian distribution of fractional occupancies is convoluted with the space lattice of the structure at specific interlamellar loci, its Fourier transform, which is also Gaussian, must be multiplied with the part of the diffraction pattern that corresponds to the order of the lamellar interface. These are just the 00*l* lamellar reflections and, hence, the often-observed attenuation of the low-angle reflections in the diffraction from any paraffin solid solution is quite simply explained. In the analyses above, only the *form* of the interfacial disorder was sought (*i.e.* an approximation of the Gaussian half-width) and not its unique description. That is to say, there may be other, similar chain-end atomic occupancies that lead to similar results. (Indeed, some have been found.) Furthermore, the conformational disorder found in vibrational spectroscopic and NMR measurements have not been considered in the above analyses, if only to avoid further complication and over-parameterization of the model. Higher precision, as shown in the X-ray structure analysis of a *n*-paraffin binary solid (Gerson & Nyburg, 1994), for example, would require more intensity data. Equivalent numbers of diffraction data are more difficult to obtain in electron crystallographic studies than in single-crystal X-ray studies, for various reasons [relative values of the form factors at high angle and also goniometric constraints (Dorset, 1995)], even though electron diffraction techniques are the most convenient to study such polydisperse solids as single crystals.

Despite the *disorder* at the lamellar interface, one surprise in this study was the very high resolution and sharpness of the reflections in the 0*kl* electron diffraction patterns from very small microareas (Fig. 1). Earlier morphological descriptions of petroleum wax crystallization (Edwards, 1957; Zocher & Machedo, 1959) led one to expect that their oriented solids would have considerable plastic deformation, perhaps of the type found for phospholipids (Dorset, Massalski & Fryer, 1987). Petroleum wax lamellae have been visualized in the light microscope as rolled up tubes, for example. The well ordered solids found on a microscale indicate, on the contrary, that the lamellar repeat must be highly correlated, despite the disorder at the lamellar interface. That is to say, even though there is a distribution of atomic occupancies at the chain ends and also a certain number of conformational defects, the lamellar surfaces

must still be very flat on an atomic scale. Furthermore, enough of an average lateral crystallographic repeat must remain on each lamellar surface to promote the exact self-epitaxial nucleation that represents the growth of one lamella on the next as a three-dimensional crystal is formed. [It will be shown in a separate paper (D. L. Dorset & B. K. Annis, in preparation), based on surface decoration experiments and AFM measurements, that this is, in fact, the case for many mixed-chain lamellar solid solutions.] The resultant minimization of nonoverlapping molecular volume is entirely consistent with the constraints imposed for solid solutions by Kitaigorodski (1961).

The beeswax structure is more difficult to characterize. First of all, it is not the stable lamellar structure found in the petroleum-based (or model) waxes, even though the chains pack in the same methylene subcell and also in rectangular layers. Comparing the diffraction patterns to earlier work on very long-chain alkanes epitaxially nucleated by a substrate from the vapor phase (Zhang & Dorset, 1990), the structure seems to be instead a 'frustrated' lamella with some nematic-like disorder of the chains. The presence of average lamellae in all areas is indicated, first of all, by the observation of low-angle $00l$ reflections (Fig. 5*c*). However, these nascent lamellae must be bridged by chains to prevent the eventual stablization of the structure found for the petroleum waxes. Such bridging would, for example, explain the occasional splitting or nonsplitting of intense $01l$ reflections (Zhang & Dorset, 1990), since the bridging molecules would constrain the interlamellar distance to some multiple of the $c_s/2 = 1.275$ Å methylene repeat (if there are many of them). Thus, as seen for partially annealed *n*-paraffins or for beeswax (Fig. 5*a*), the most intense reflections resemble the electron diffraction patterns from polyethylene (*e.g.* see Hu & Dorset, 1989). A partial relaxation of this interlamellar distance to a nonintegral multiple of the methylene repeat distance (if there are fewer bridges) means that the original nascent lamellar structure is now better defined. As found for more completely annealed *n*-$C_{60}H_{122}$ and also for beeswax (Fig. 5*b*), the intense $01l$ reflections are now split but not the outer $00l$ reflections. However, the unusual index rule found for the $01l$ reflections indicates that the analogy to the earlier study of very long alkanes is not exact. Some component of the very complicated list of beeswax ingredients, perhaps the long-chain diol diesters (Stransky, Streibl & Kubelka, 1971), is responsible for this structure remaining in a permanently unresolved state. The endpoint of annealing the oriented long paraffins is a stable lamella (Zhang & Dorset, 1990) with flat surfaces, but this cannot be formed for the insect wax for reasons that are not yet clear.

Research was supported in part by grants from the National Science Foundation (CHE91-13899 and CHE94-17835), which are gratefully acknowledged. Time on the high-voltage electron microscope was supported by Biotechnological Resource grant RR01201, awarded by the National Center for Research Resources, Department of Health and Human Services/ Public Health Service to support the Wadsworth Center of the NY State Department of Health's Biological Microscopy and Image Reconstitution Facility as a National Biotechnological Resource. Dr W. F. Tivol is especially thanked for technical assistance during data collection on this instrument. Thanks are also due to Dr W. A. Pangborn for obtaining a low-angle X-ray pattern from the beeswax. Mr Jon Weekly of Mahoney and Weekly Booksellers is thanked for the gift of the beeswax. Dr Ilsa Basson is thanked for productive discussions.

References

ABRAHAMSSON, S., DAHLÉN, B., LÖFGREN, H. & PASCHER, I. (1978). *Prog. Chem. Fats Other Lipids*, **16**, 125–143.

ALEBY, S., FISCHMEISTER, I. & IYENGER, B. T. R. (1971). *Lipids*, **6**, 421–425.

ASBACH, G. I. & KILIAN, H. G. (1991). *Polymer*, **32**, 3006–3012.

ASBACH, G. I., GEIGER, K. & WILKE, W. (1979). *Colloid Polym. Sci.* **257**, 1049–1059.

BASSON, I. & REYNHARDT, E. C. (1988). *J. Phys. D*, **21**, 1421–1428.

BASSON, I. & REYNHARDT, E. C. (1991). *J. Chem. Phys.* **95**, 1215–1222.

BASSON, I. & REYNHARDT, E. C. (1992). *J. Chem. Phys.* **97**, 1287–1295.

COWLEY, J. M., REES, A. L. G. & SPINK, J. A. (1951). *Proc. Phys. Soc. (London) A*, **64**, 609–619.

CRAIEVICH, A., DOUCET, J. & DENICOLO, I. (1984). *J. Phys. (Paris)*, **45**, 1473–1477.

DORSET, D. L. (1976). *Acta Cryst.* A**32**, 207–215.

DORSET, D. L. (1987). *Macromolecules*, **20**, 2782–2788.

DORSET, D. L. (1990*a*). *Proc. Natl. Acad. Sci. USA*, **87**, 8541–8544.

DORSET, D. L. (1990*b*). *Macromolecules*, **23**, 623–633.

DORSET, D. L. (1994). *Adv. Electron. Electron Phys.* **88**, 111–197.

DORSET, D. L. (1995). *Structural Electron Crystallography*. New York: Plenum Press. In the press.

DORSET, D. L. & HAUPTMAN, H. A. (1976). *Ultramicroscopy*, **1**, 195–201.

DORSET, D. L. & ZEMLIN, F. (1990). *Ultramicroscopy*, **33**, 227–236.

DORSET, D. L. & ZHANG, W. P. (1991). *J. Electron Microsc. Tech.* **18**, 142–147.

DORSET, D. L., ALAMO, R. G. & MANDELKERN, L. (1992). *Macromolecules*, **25**, 6284–6288.

DORSET, D. L., HANLON, J. & KARET, G. (1989). *Macromolecules*, **22**, 2169–2176.

DORSET, D. L., HU, H. & JÄGER, J. (1991). *Acta Cryst.* A**47**, 543–549.

DORSET, D. L., MASSALSKI, A. K. & FRYER, J. R. (1987). *Z. Naturforsch. Teil A*, **42**, 381–391.

DOWNING, D. T., KRANZ, Z. H., LAMBERTON, J. A., MURRAY, K. E. & REDCLIFFE, A. H. (1961). *Aust. J. Chem.* **14**, 253–263.

DOYLE, P. A. & TURNER, P. S. (1968). *Acta Cryst.* B**24**, 390–397.

EDWARDS, R. T. (1957). *Ind. Eng. Chem.* **49**, 750–757.

FISCHER, E. W. (1971). *Pure Appl. Chem.* **26**, 385–421.

GERSON, A. R. & NYBURG, S. C. (1994). *Acta Cryst.* B**50**, 252–256.

HU, H. & DORSET, D. L. (1989). *Acta Cryst.* B**45**, 283–290.

HU, H., DORSET, D. L. & MOSS, B. (1989). *Ultramicroscopy*, **27**, 161–170.

KIM, Y., STRAUSS, H. L. & SNYDER, R. G. (1989). *J. Phys. Chem.* **93**, 485–490.

KITAIGORODSKII, A. I. (1961). *Organic Chemical Crystallography*, pp. 230–240. New York: Consultants Bureau.

LÜTH, H., NYBURG, S. C., ROBINSON, P. M. & SCOTT, H. G. (1974). *Mol. Cryst. Liq. Cryst.* **27**, 337–357.
MARONCELLI, M., STRAUSS, H. L. & SNYDER, R. G. (1985). *J. Phys. Chem.* **89**, 5260–5267.
MNYUKH, YU. V. (1960). *Zh. Strukt. Khim.* **1**, 370–388.
NYBURG, S. C. & POTWOROWSKI, J. A. (1973). *Acta Cryst.* B**29**, 347–352.
PIESCZEK, W., STROBL, G. R. & MALZAHN, K. (1974). *Acta Cryst.* B**30**, 1278–1288.
STRANSKY, K. & STREIBL, M. (1971). *Collect. Czech. Chem. Commun.* **36**, 2267–2280.
STRANSKY, K., STREIBL, M. & KUBELKA, V. (1971). *Collect. Czech. Chem. Commun.* **36**, 2281–2297.
TEGELAAR, E. W., MATTHEZING, R. M., JANSEN, J. B. H., HORSFIELD, B. & DE LEEUW, J. W. (1989). *Nature*, **342**, 529–531.
TULLOCH, A. P. (1970). *Lipids*, **5**, 247–258.
TULLOCH, A. P. (1971). *Chem. Phys. Lipids*, **6**, 235–265.
TULLOCH. A. P. (1972). *J. Am. Oil Chem. Soc.* **49**, 609–610.
TULLOCH, A. P. & HOFFMAN, L. L. (1972). *J. Am. Oil Chem. Soc.* **49**, 696–699.
WITTMANN, J. C., HODGE, A. M. & LOTZ, B. (1983). *J. Polym. Sci., Phys. Ed.* **21**, 2495–2509.
ZHANG, W. P. & DORSET, D. L. (1990). *J. Polym. Sci. B. Polym. Phys.* **28**, 1223–1232.
ZOCHER, H. & MACHADO, R. D. (1959). *Acta Cryst.* **12**, 122–125.

Acta Cryst. (1995). B**51**, 1028–1035

Structure Determination of Organic Compounds Using an In-Laboratory Rapid X-ray Measurement System – Comparison with Structures Determined by a Four-Circle Diffractometer

BY FUJIKO IWASAKI,* MASAHIRO SAKURATANI, HAJIME KANEKO AND MASANORI YASUI

Department of Applied Physics and Chemistry, The University of Electro-Communications, Chofu-shi, Tokyo 182, *Japan*

AND NOBUO KAMIYA AND HITOSHI IWASAKI

The Institute of Physical and Chemical Research (RIKEN), Wako-shi, Saitama 351-01, *Japan*

(*Received* 17 *August* 1993; *accepted* 22 *May* 1995)

Abstract

A new type of X-ray diffractometer (IPD-WAS) has been recently developed as a rapid X-ray measurement system in the laboratory. This equipment has been closely examined from the viewpoint of a tool for the data collection of organic crystals. Intensities of two stable compounds [I: bis(2,4,6-trimethylthiobenzoic) thioanhydride; II: dimethyl 1,2-di-*tert*-butyl-3,6-dimethyl 4,5-dicarboxylate] and one unstable compound (III: tri-4-methylphenylbismuth dichloride) were measured with Mo $K\alpha$ radiation, with the total time for the intensity measurement being 2 or 3 h for each compound. 1995, 2360 and 2502 independent reflections of 3520, 5238 and 5397 measured reflections were used for structure determination for (I), (II) and (III), respectively. The structures were solved successfully by conventional direct methods and the Patterson method. The final R values were 0.055, 0.050 and 0.067 for (I), (II) and (III), respectively. For (I) and (II), intensities were also measured with a four-circle diffractometer using the same specimens, the final R values being 0.058 and 0.055 for 2733 and 3224 reflections for (I) and (II), respectively. The agreement between the two sets of structural geometry, obtained from the IPD-WAS and the four-circle diffractometer, was quite satisfactory. Accurate intensities of the unstable (III) could not be obtained by the four-circle diffractometer.

1. Introduction

Rapid collection of X-ray intensity data is especially important for determining structures of unstable compounds. In order to obtain an intensity data set from a single crystal within several hours, a new type of X-ray diffractometer, IPD-WAS (Kamiya, Iwasaki, Tanaka & Katayama, 1990; Kamiya, Iwasaki & Tanaka, 1993; Kamiya & Iwasaki, 1995), was recently developed for time-resolved data collection of intermediate states of crystalline-phase reactions. IPD-WAS consists of a rotating anode generator and a focusing monochromator, a chamber containing a Weissenberg camera with multi-screens which are automatically adjustable to any desired layer lines for lowering background level, two cylindrical imaging plates (Amemiya & Miyahara, 1988; Sonoda, Takano, Miyahara & Kato, 1983) as two-dimensional detectors, which are used alternately to reduce effective readout time for each imaging plate, and a rotating laser optics newly designed for the readout of the cylindrical

* Author to whom all correspondence should be addressed.